I

Paper I

K. M. Laundal and N. Østgaard (2008)

Persistent global proton aurora caused by high solar wind dynamic pressure

Journal of Geophysical Research Vol. 113, doi:10.1029/2008JA013147

© 2008 American Geophysical Union

JOURNAL OF GEOPHYSICAL RESEARCH, VOL. 113, A08231, doi:10.1029/2008JA013147, 2008

Click Here for Full Article

Persistent global proton aurora caused by high solar wind dynamic pressure

K. M. Laundal[1] and N. Østgaard[1]

Received 6 March 2008; revised 1 May 2008; accepted 9 May 2008; published 28 August 2008.

[1] Global images of the proton aurora taken with the SI-12 camera onboard the IMAGE satellite reveal a very direct relationship between the solar wind dynamic pressure and the intensity of the global proton aurora. We show that an increase in dynamic pressure leads to an immediate and persistent increase in proton precipitation, also when the increase is slow. When the dynamic pressure decreases, the proton aurora diminishes. Five events during geomagnetic quiet times, with mostly northward IMF, have been selected in order to characterize the proton aurora caused exclusively by high dynamic pressure and establish important criteria that the dynamic pressure-induced precipitation mechanism(s) must satisfy. We also present measurements during southward IMF and show that the combined effect of high solar wind dynamic pressure and southward IMF produces intense global proton aurora. Some of the characteristics are: (1) The aurora is global, with peak intensities at midnight and flanks. (2) A dawn/dusk asymmetry shows that the precipitation originates from magnetospheric protons that have undergone gradient/curvature drift. (3) The time delay between ground magnetic signatures of a change in the solar wind dynamic pressure and a change in global proton aurora is short (−2 minutes). Our observations indicate that the precipitation mechanism(s) behind the proton aurora during high dynamic pressure is directly connected to the compression of the magnetosphere, both at the flanks and nightside.

Citation: Laundal, K. M., and N. Østgaard (2008), Persistent global proton aurora caused by high solar wind dynamic pressure, *J. Geophys. Res.*, *113*, A08231, doi:10.1029/2008JA013147.

1. Introduction

[2] The solar wind dynamic pressure is an important parameter for controlling the shape and size of the magnetosphere. A sudden increase in dynamic pressure can cause global disturbances in the magnetosphere, which are accompanied by an increase of the intensity of the aurora [*Vorobyev*, 1974; *Craven et al.*, 1986; *Spann et al.*, 1998; *Zhou and Tsurutani*, 1999; *Zhou et al.*, 2003]. Recent studies, using global images from space, have shown that the auroral intensifications appear first at the dayside and propagate to the nightside at an ionospheric speed consistent with the speed of the solar wind discontinuity [*Zhou and Tsurutani*, 1999], at least when the dynamic pressure pulse is preceded by a period with northward IMF [*Boudouridis et al.*, 2003]. These transient intensifications are often referred to as shock auroras, since they are believed to be caused by the sudden magnetospheric reconfiguration due to the sudden increase of solar wind pressure. *Liou et al.* [2006] showed that a negative sudden impulse in solar wind dynamic pressure leads to a fast, global reduction in auroral intensity.

[3] The effect of a long-lasting high solar wind dynamic pressure on the aurora has been much less studied. *Zhou and Tsurutani* [2003] showed that the auroral intensity at dawn and dusk, seen by the UVI camera on the Polar satellite, increased (decreased) during gradually increasing (decreasing) dynamic pressure. Using the same camera, *Liou et al.* [2007] showed that the global auroral luminosity is higher when the magnetosphere is compressed, leading to the term "compression aurora". They also found, using in situ DMSP measurements, that most of the auroral emissions during compression were due to diffuse electron precipitation.

[4] The production mechanism for the persistent aurora during high dynamic pressure is believed to differ from the transient mechanisms behind the shock aurora. *Zhou and Tsurutani* [2003] suggested that the dawn and dusk aurora could be due to Kelvin–Helmholtz waves on the magnetopause. *Liou et al.* [2007] suggested that the increased intensity is due to a larger loss cone caused by a decrease in the mirror ratio, B_m/B_{eq}, since the equatorial magnetic field strength, B_{eq} increases more than at the mirror points, B_m, during compression.

[5] The first, and so far only camera with the ability to look at the global aurora solely produced by protons, is the SI-12 camera [*Mende et al.*, 2000] on board the IMAGE satellite. Using this ability, *Meurant et al.* [2003, 2004] showed that a sudden increase in the solar wind dynamic pressure affects both electron and proton precipitation however with some differences in timing and distribution. *Coumans et al.* [2006] showed in a statistical study, that the

[1]Department of Physics and Technology, University of Bergen, Bergen, Norway.

Copyright 2008 by the American Geophysical Union.
0148-0227/08/2008JA013147$09.00

total power of the proton precipitation was correlated with the solar wind dynamic pressure. The slope in the regression line between dynamic pressure and proton precipitation energy flux was highest near midnight and higher in the summer than in the winter.

[6] In this paper we look at the lasting effect of a change in solar wind dynamic pressure on the global proton aurora, seen by the SI-12 camera. We show that high dynamic pressure leads to a persistent intense proton aurora. We look at five events during geomagnetic quiet times, in order to establish some characteristics of the dynamic pressure induced aurora, that a production mechanism must account for. The quiet times are chosen to avoid contributions from other processes, such as substorms and convection caused by southward IMF, and the magnetosphere can be assumed to be in a quasisteady state. Although the effect of the dynamic pressure is clearly seen in the quiet time measurements, the aurora is faint. Two events with southward IMF are also studied, and we show that a combination of southward IMF and high solar wind dynamic pressure may be decisive parameters for generation of intense proton precipitation.

[7] In section 2, the observations are presented. Section 3 contains a discussion of possible production mechanisms induced by the high solar wind dynamic pressure, in relation to our observations. Section 4 contains the conclusions.

2. Observations

[8] The SI-12 camera [*Mende et al.*, 2000] has a narrow passband with peak sensitivity at 121.8 nm and block-out of the Hydrogen emission line at 121.567 nm (Ly-α). Hence only Doppler shifted Ly-α emissions are detected. Such emissions are produced by Hydrogen descending at a sufficiently high speed along the line of sight. This Hydrogen is in turn produced by proton precipitation which charge exchange with atmospheric constituents. Only protons with energy above 1 keV can produce detectable emissions [*Mende et al.*, 2003]. Above this threshold, the sensitivity of the SI-12 camera is highest at 3–4 keV for an isotropic distribution of protons and decreases with increasing energy [*Frey et al.*, 2003].

[9] The relation between an instrument count in SI-12 and a physical quantity such as energy flux or number flux requires that, e.g., the mean energy of the precipitation is known [*Gérard et al.*, 2001; *Frey et al.*, 2003]. Since global measurements of the mean energy are not available, statistical maps [*Hardy et al.*, 1989] are often used. However, in this paper, we focus on proton aurora produced by a mechanism induced by high solar wind dynamic pressure, which may produce different energy spectra than other mechanisms. Since assumptions based on statistical maps of proton precipitation may introduce artificial inaccuracies, we will avoid the use of energy flux and present the SI-12 data in corrected instrument counts (instrument calibration is described in *Frey et al.* [2003]). We use the terms "instrument counts" and "proton aurora intensity" interchangeably. A constant background of 4 counts/pixel, and a variable crescent shaped dayglow, has been subtracted from each image. The time resolution of the SI-12 camera is approximately 2 minutes (one satellite spin period), and the integration time is 5 seconds.

[10] For measurements of the solar wind and IMF, we use the ACE satellite, located near the Lagrange point at $x_{GSM} \sim 250\ R_E$. To determine the timing of the solar wind arrival to the magnetopause (taken as 10 R_E), we time-shift each data point by s/v, where s is the distance along the GSM x direction to the ACE satellite. We then adjust the time-shift so that solar wind dynamic pressure discontinuities coincide with abrupt changes in the SYM-H index. The SYM-H index is derived from low latitude ground magnetometer measurements, and can be seen mainly as a one minute equivalent to the Dst index [*Wanliss and Showalter*, 2006], and is sensitive to changes in the ring current, but also has a contribution from the magnetopause current [e.g., *Burton et al.*, 1975]. Thus we have an accurate time, within the one minute time resolution of SYM-H and the ACE measurements, for the arrival of the discontinuity at the magnetopause, while the timing for other solar wind data points may be slightly dislocated in time.

2.1. Five Quiet Time Dynamic Pressure Events

[11] In Figures 1a–1e, we show five events with quiet geomagnetic conditions, to avoid any superimposed effects of processes independent of the solar wind dynamic pressure. All events in this study are from 2001, when the $\sim$7 R_E apogee of the IMAGE satellite was close to the north pole, which enabled continuous observation of the area above 50° magnetic latitude for several hours per 14 hour orbit.

2.1.1. 21–22 April 2001

[12] Figure 1a shows the end of a long period with high dynamic pressure. The positive direction of the IMF B_z (bottom) indicates low geomagnetic activity. The AE indices (not shown) also showed low activity at this time. The third panel from the top shows that the solar wind dynamic pressure first increases at 23:35 UT, and then quickly decreases just before 00:40 UT. The dynamic pressure reduction is accompanied by a fast drop in proton aurora intensity. In the more than 1 hour long period with SI-12 data prior to the drop in dynamic pressure, the MLT keogram (top) shows two steady maxima in aurora intensity at dusk, centered approximately at 18 MLT, and at dawn, centered at approximately 4 MLT. The dusk aurora is more intense than at dawn.

[13] The fourth panel from the top shows the solar wind velocity (black) and density. When the dynamic pressure decreases, at 00:40 UT, the solar wind velocity increases. The drop in dynamic pressure is caused by a large decrease in density, from approximately 40 to 10 cm^{-3}. The relative changes in density and velocity are important for various proposed production mechanisms, such as Kelvin–Helmholtz (K–H) waves on the magnetopause [*Zhou and Tsurutani*, 2003], which will be discussed in section 3.

[14] In the top panel of Figure 2a, we have plotted the correlation coefficients between the proton aurora intensity and solar wind dynamic pressure at different magnetic local times for the 21–22 April event. The intensity of the proton aurora depends on the state of the magnetosphere, which may have a highly delayed response to changes in the solar wind and the IMF. Hence consecutive measurements by the SI-12 camera, spaced by only 2 minutes, are not statistically independent. This means that even though the correlations presented in Figure 2 are based on a large number of

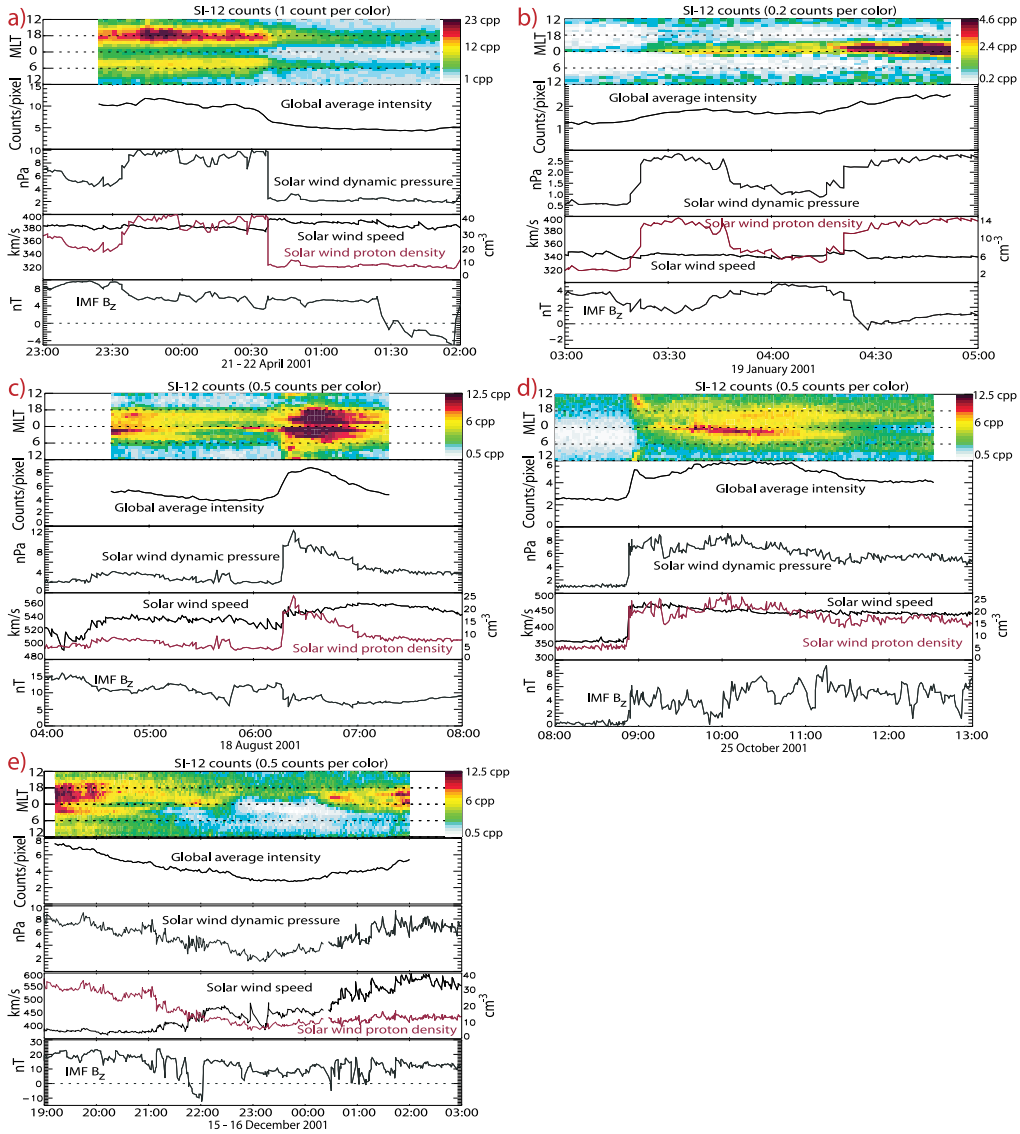

Figure 1. The panels show, from top to bottom: (1) MLT keogram. Each pixel represents 1 hour magnetic local time, integrated from 60 to 85° magnetic latitude. The unit on the color bars is counts per pixel (cpp). (2) Global average proton aurora intensity, measured in corrected instrument counts/pixel in the area between 60 and 85 degrees magnetic latitude. (3) Time-shifted solar wind dynamic pressure. (4) Solar wind velocity (black) and density (red). (5) IMF B_z. Note that the scales vary.

samples, one should be careful in concluding about the true correlation, since the significance of the correlation coefficients is much less than they would be if the data were obtained with larger time intervals. However we shall use the calculated correlation coefficients only as a measure of how well the data in each particular event vary together, and look at the differences between magnetic local times. The top panel of Figure 2a shows a clear pattern, with higher correlation at dawn and dusk, than at midnight and noon. In the bottom panel, we have used data points only from the period prior to the dynamic pressure decrease at 00:40 UT, to look at the common variation without the effect of the

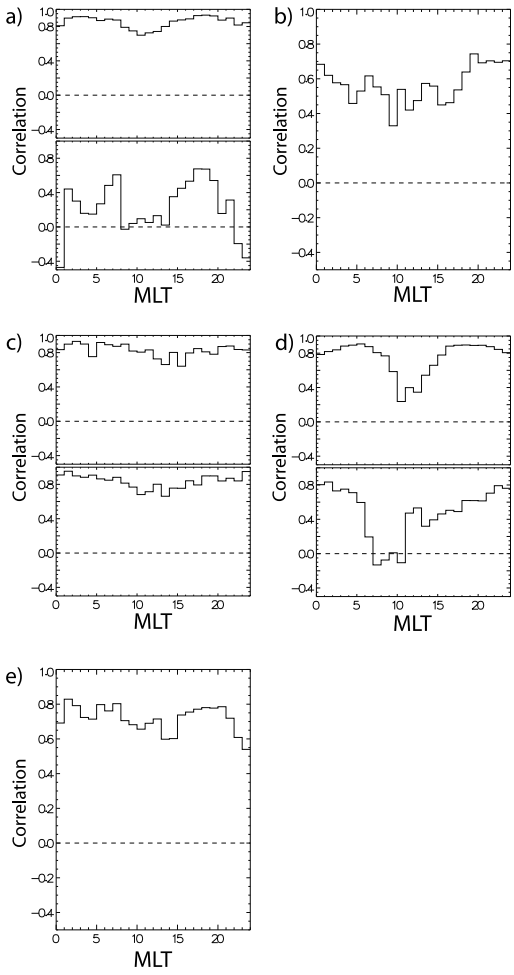

Figure 2. The calculated correlation coefficients between solar wind pressure and proton aurora intensity at different MLTs for the events in Figure 1. (a) 21–22 April, (b) 19 January, (c) 18 August, (d) 25 October, (e) 15–16 December, all from 2001. The bottom panels show the correlation without pressure discontinuity.

large dynamic pressure drop. We see that the correlation is lower at all local times, as expected, but the >0.6 correlation seen on the dusk side suggests that also the small changes in solar wind dynamic pressure affect the proton aurora. This is confirmed by the MLT keogram, which shows an increase in the dusk aurora intensity in response to the dynamic pressure increase at 23:35 UT.

2.1.2. 19 January 2001

[15] Figure 1b shows data from 19 January 2001. A dynamic pressure increase from 0.5 to 2.5 nPa is seen at 03:20 UT. The MLT keogram shows a small increase in intensity mainly at the nightside (note the greatly reduced color scale from the previous event). Between 03:50 and 04:20 the dynamic pressure is down to 1 nPa, and then it rises again to 2–2.5 nPa. At the time of this second dynamic pressure increase, the auroral intensity increases again, to a higher value than in the first increase. The IMF B_z was northward (≈3–4 nT) for approximately two hours prior to the second dynamic pressure increase, when it became ≈0 nT. This turning of the IMF may be the reason for the higher proton aurora intensity at this time.

[16] This example illustrates that the solar wind dynamic pressure has a clear effect on the proton aurora, also for relatively low values. Whether or not these observations are a consequence of the abrupt increase, or an effect of persistent high dynamic pressure, is unclear, due to the relatively short duration of the first dynamic pressure pulse.

[17] The aurora was very faint at all MLTs in this event, only a few counts higher than the background. However, compared to other MLTs, the correlation between dynamic pressure and aurora intensity was high on the pre midnight MLTs (Figure 2b).

2.1.3. 18 August 2001

[18] Figure 1c shows proton aurora measurements from 18 August 2001. This is the late recovery phase of a geomagnetic storm, but the geomagnetic conditions are otherwise quiet: no substorms are detected, and the IMF B_z is strictly positive. At approximately 06:15 UT we see a sudden increase in dynamic pressure, which results in an intensification of the proton aurora at all magnetic local times. The most intense proton aurora is found on the nightside. During the subsequent hour, both the dynamic pressure and the proton aurora intensity decreases.

[19] The top panel of Figure 2c shows the correlation between solar wind dynamic pressure and proton aurora intensity at different magnetic local times. The bottom panel shows the correlation only in the period starting 20 minutes after the increase in solar wind dynamic pressure. The high correlation seen in both cases indicates that the dynamic pressure controls the proton aurora at all times.

2.1.4. 25 October 2001

[20] Figure 1d shows the response in proton aurora intensity to a sudden increase in solar wind dynamic pressure, followed by a 3.5 hours long period with slowly varying, high dynamic pressure. In the ~20 minutes following the sudden increase in dynamic pressure, the proton aurora intensifies on the dayside, and travels anti-sunward, mainly along the dusk flank. This is consistent with the description of the proton aurora caused by a sudden increase in dynamic pressure described by *Meurant et al.* [2004]. According to *Frey et al.* [2004], there was a substorm onset at 09:09:56 UT, located at 23:26 MLT. The local intensification seen at this time and location in the MLT keogram may be due to this possibly pressure triggered substorm. It should be mentioned that we have seen no substorm signatures in ground magnetometer data in this event. In the last ~2 hours with SI-12 data, the aurora is located mainly at the flanks, with a similar configuration as the 22 April event (Figure 1a).

[21] Figure 2d shows the correlation between proton aurora intensity and solar wind dynamic pressure at different local times for the whole time interval (top) and the period starting 20 minutes after the solar wind dynamic pressure increase (bottom). As discussed above, the inten-

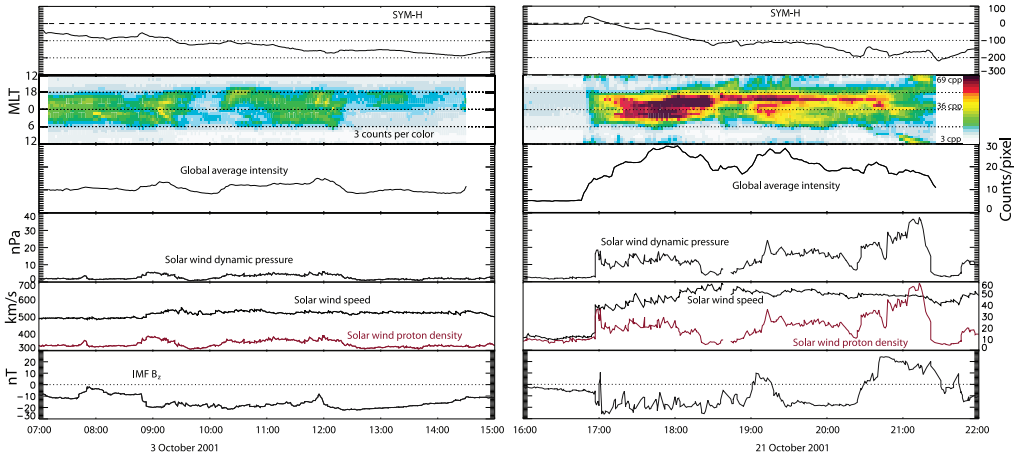

Figure 3. 3 October (left) and 21 October (right), 2001. The panel show, from top to bottom: (1) SYM-H [nT], a similar index as the Dst, with 1 minute resolution. (2) MLT keogram (note the crude color scale, due to the high intensity in these events). (3) Global average proton aurora intensity ($\geq$50 magnetic latitude). (4) Solar wind dynamic pressure. (5) Solar wind velocity (black) and density (red). (6) panel: IMF B_z.

sity in this event may have been affected by a substorm. However it is not believed that the substorm was equally important at all local times, and we see a similar pattern here as in the event from April 2001, with higher correlation on the flanks, and lower correlation on the dayside. The bottom panel shows that the correlation is lower without the transient effect of the sudden increase in dynamic pressure, but it is still high at the nightside and flanks, compared to the dayside.

2.1.5. 15–16 December 2001

[22] Figure 1e shows an event from 15 December 2001 when the dynamic pressure decreased slowly from $\approx$9 to $\approx$2 nPa over 4 hours, and then increased again. This was also the case for the proton aurora intensity, which started at an average of 7 counts, decreased to 3 counts, and increased to 5 counts again. In the first 70 minutes, the proton aurora was primarily located in an $\approx$3 hours wide MLT sector in the post midnight sector, and a much wider area at dusk. The dusk aurora is visible throughout the period. The IMF B_z was positive or close to zero during the whole event, except for a period of $\approx$15 minutes around 22:00 UT, when it turned southward. This is probably the reason for the seen in the MLT keogram near midnight brief intensification at this time.

[23] Due to the absence of large discontinuities in the solar wind, this event demonstrates one of our main points: High solar wind dynamic pressure leads to an enhanced proton aurora intensity, also when the solar wind dynamic pressure changes slowly (or not at all).

[24] The correlation between solar wind dynamic pressure and proton aurora intensity (Figure 2e) is quite high at all magnetic local times in this event, including the dayside. The minimum seen between 23 and midnight can probably be explained by the fact that the intensity at this local time was low, except for the 15 minutes with southward IMF.

2.2. Solar Wind Dynamic Pressure Control of High Intensity Proton Aurora

[25] So far we have looked only at events when the IMF was mostly northward. Many previous studies show that changes in solar wind dynamic pressure have much more dramatic consequences when it is combined with southward IMF [e.g., *Meurant et al.*, 2004; *Lee and Lyons*, 2004; *Boudouridis et al.*, 2004; *Lee et al.*, 2007], and we want to see if this holds also for the proton aurora intensity.

[26] Figure 3 shows data from two geomagnetic storm main phases, characterized by steep decreases in SYM-H, a signature of significant injection of energy into the ring current. It is believed that an increase of ring current energy is associated with injection of protons of isotropic pitch angle distribution, which is a major cause for precipitation [*Søraas et al.*, 2002; *Mende et al.*, 2002]. The similarity in the magnitude of the drop in SYM-H suggests that the events in Figure 3 are to some extent comparable in terms of injection of isotropic protons.

[27] There are however big differences in the proton aurora intensity: On 21 October 2001, the intensity (Third panel from the top) was approximately a factor of 2 higher than 3 October. Note that the color scale in the MLT keogram (second panel) has been adjusted to 3 counts per color due to the high intensity, and that we look at the entire region poleward of 50° magnetic latitude, due to the expansion of the auroral oval. The axis and color scales are the same for both events in Figure 3.

[28] The solar wind data shows that the IMF B_z (bottom panel) was negative, and had a similar magnitude in the two events. The dynamic pressure (fourth panel from the top) was however much higher on 21 October than it was on 3 October. This indicates that the difference in dynamic pressure is the reason for the large difference in proton aurora intensity. A one-to-one relationship between solar

wind dynamic pressure and proton aurora intensity cannot be claimed when so many processes are present that can cause precipitation. However we also see that the periods with the most intense aurora in both events coincided with the periods when the dynamic pressure was highest. An exception to this is found at the end of the 21 October event, when the dynamic pressure reached very high values (>30 nPa), with a relatively faint nightside aurora. This can probably be explained by the fact that the IMF B_z had turned northward. The keogram shows that most of the intensity in this period is located on the dayside.

[29] Figure 3 indicates that high solar wind dynamic pressure or southward IMF alone are not able to produce proton aurora with very high intensity. A combination of high dynamic pressure and southward IMF may however be a necessary and sufficient criterion for high intensity proton aurora. This is in accordance with the statistical study by *Coumans et al.* [2006], who found that the slope of the linear regression line for proton aurora power and solar wind dynamic pressure was higher during southward IMF.

3. Discussion

[30] The observations presented in this paper show that a change in solar wind dynamic pressure is reflected in the global proton aurora intensity. The mechanism(s) responsible for this relationship must account for several characteristics: (1) Persistent high dynamic pressure leads to a persistent high proton aurora intensity. This is the reason that we believe the mechanism(s) behind the proton aurora observed in this study differ from the mechanisms behind the transient shock aurora. (2) The time delay between a change in ground magnetic field signatures of a change in solar wind dynamic pressure, both positive and negative, and a change in proton aurora intensity is very short, possibly below the 2 minutes time resolution of the SI-12 images. (3) Some events (22 April and the end of 25 October) showed that the dynamic pressure induced aurora was predominantly located at the flanks, but this is not always seen (18 August, 19 January). (4) The dawn/dusk asymmetry shows that the aurora originates from magnetospheric protons that have undergone gradient/curvature drift, and precipitate due to some mechanism induced by the high dynamic pressure. This is consistent with *Liou et al.* [2007], who reported a similar pattern in the electron dominated aurora caused by high dynamic pressure, only with the highest intensity at dawn. (5) The intensification of the proton aurora during high dynamic pressure is seen regardless of the sign of the IMF B_z. However a much more dramatic effect of high solar wind dynamic pressure is seen when the IMF is southward (Figure 3) than when it is northward, consistent with many reports on the effect of dynamic pressure on the magnetosphere.

[31] The two theories used to explain the energy transfer from the solar wind to the magnetosphere are reconnection [*Dungey*, 1961], which is least efficient when IMF $B_z > 0$, and viscous interaction [*Axford and Hines*, 1961], which can be independent of the sign of B_z. We have shown five events where high dynamic pressure led to increased precipitation, even though the IMF was northward, which may be taken as a sign of viscous interaction. One possible viscous interaction mechanism is Kelvin–Helmholtz waves on the magnetopause flanks, which agrees with the flank location of the aurora seen in Figure 1a and at the end of the 25 October event (Figure 1d). This was the argument of *Zhou and Tsurutani* [2003], who observed dynamic pressure dependent flank auroras using the Polar UVI camera, which is sensitive mainly to electron produced auroral emissions.

[32] The onset condition for K–H waves is [e.g., *Baumjohann and Treumann*, 1997]

$$(\mathbf{k}\cdot\Delta\mathbf{v})^2 > \frac{n_1+n_2}{m_p\mu_0 n_1 n_2}\left((\mathbf{k}\cdot\mathbf{B}_1)^2+(\mathbf{k}\cdot\mathbf{B}_2)^2\right) \quad (1)$$

where subscripts 1 and 2 denote the regions outside and inside the magnetopause, respectively. **B** is the magnetic field, n is the plasma density, **k** is the wave vector, and $\Delta\mathbf{v}$ is the shear velocity across the magnetopause. The inequality 1 shows that the shear velocity is a more important parameter in controlling K–H wave growth than the plasma density. Hence K–H wave activity is much more sensitive to changes in solar wind velocity, than density [e.g., *Engebretson et al.*, 1998]. In the 21–22 April event (Figure 1a), the proton aurora (and solar wind dynamic pressure) was clearly governed by changes in solar wind density, with an increasing solar wind velocity at the time of the drop in dynamic pressure. The 19 January event (Figure 1b) also showed a clear response to an increase in density, with a nearly constant velocity. The first period of the 15–16 December event (Figure 1e) had high solar wind density, while the last period had high velocity, with no apparent difference in the dynamic pressure control of the overall proton aurora intensity. These examples illustrate that it is the combined effect of the solar wind velocity and density, namely the dynamic pressure, $P = m_p n v^2$, and not the velocity in particular, that governs the global proton aurora, as would be expected if Kelvin–Helmholtz waves was the driving mechanism.

[33] A more direct mechanism was proposed by *Liou et al.* [2007], who observed persistent increased intensity in the electron-dominated aurora seen by Polar UVI during high solar wind dynamic pressure. They suggest that the increased intensity is caused by a decrease in the mirror ratio, B_m/B_{eq}, since the equatorial magnetic field increases most during compression, leading to a larger loss cone.

[34] Many of the features in the observations presented in this paper support the idea that the dynamic pressure induced aurora follows directly from the compression of the magnetosphere. A quick compression/expansion of the magnetosphere following a change in the solar wind dynamic pressure quickly turns on or off the precipitation mechanism, in agreement with, e.g., the observations in Figure 1d (on) and Figure 1a (off). However it is not clear why a reduced mirror ratio should lead to maxima at the flanks, and in particular why there is a higher intensity at the dawn sector than at noon, where the magnetosphere gets much more compressed than other MLTs. Another problem is that an increase in the size of the loss cone intuitively would lead to a short-lived intensification, lasting long enough for the protons within the loss cone to be emptied; only a few minutes, considering the bounce periods of >1 keV protons. This means that a continuous supply of new protons, or an acceleration of "old" protons is needed to explain the persistent high intensity. An explanation for

both the flank location and the persistence of proton aurora may be increased magnetospheric convection triggered by the compression [*Lukianova*, 2003; *Boudouridis et al.*, 2004, 2005, 2008]. In a steady state, charged particles from the tail cannot enter closed trajectories (the symmetric ring current), and are led around the Earth, to the flanks, with a larger fraction of the protons at the dusk flank due to magnetic field gradient and curvature drifts. At the flanks, the particles encounter a more compressed magnetic field, and some precipitate. Particles that are not on closed trajectories are convected out in the magnetosheath, and are lost from the magnetosphere. *Shue et al.* [2002] studied global electron aurora, driven by convection, located primarily on the flanks (two-cell aurora) during substorm growth phase. The strikingly similar distribution observed in the compression aurora events presented by *Liou et al.* [2007], and the distribution (with opposite asymmetry) in the proton aurora events shown in Figures 1a and 1d, further support the suggestion that convection plays a role in the generation of the aurora during high pressure.

[35] *Anderson and Hamilton* [1993] reported onset (cessation) of electromagnetic ion cyclotron waves (EMIC) in the magnetosphere in response to a contracting (expanding) magnetosphere. These waves are believed to result from the increased energy anisotropy of magnetospheric protons during compression. Interaction with EMIC waves is a possible acceleration mechanism, scattering protons into the loss cone.

[36] While the aurora in Figure 1a was primarily located at the flanks, other events have a maximum located near midnight. This is most clearly seen in Figures 1b and 1c. The different locations may suggest different precipitation mechanisms. One possible mechanism at the nightside is pitch angle scattering in areas with small magnetic field line curvature radius. If a particle with gyro radius r_g encounters an area where $\frac{R_c}{r_g} \lesssim 8$, where R_c is the field line curvature, the particles can be scattered into the loss cone due to violation of the first adiabatic invariant [*Sergeev et al.*, 1983]. This is most likely to happen on the stretched magnetic field lines on the nightside magnetosphere. A study by *Boudouridis et al.* [2008] indicates that a sudden increase in dynamic pressure induces enhanced magnetotail reconnection. The resulting newly closed field lines would have a very small curvature, and so could contribute to pitch angle scattering.

[37] *Lee et al.* [2007] studied the response of ENAs to solar wind dynamic pressure variations, and found that the flux of ENAs exhibits a global increase (decrease) in response to magnetospheric compression (decompression). They claim that this behavior is due to adiabatic energization, with a reinforcing effect from the inward motion of the charged particles to areas where the density of neutral atoms is higher. One of the events studied by *Lee et al.* [2007] was the 18 August 2001 event. The flux of <10 keV energetic neutral hydrogen in this event showed a very similar development as the global average proton aurora intensity (Figure 1c). However the relative increase in <10 keV hydrogen was less than 30%, while the global proton aurora increased by ≈100% from the intensity prior to the dynamic pressure increase. The similarity in the time development of ENA emissions and proton aurora intensity may suggest a production mechanism of common origin during high solar wind dynamic pressure. However the large discrepancy in the relative changes in the 18 August event indicates that adiabatic energization is not sufficient to account for the entire increase in proton aurora without some additional mechanism.

4. Conclusions

[38] We have shown that (1) High solar wind dynamic pressure leads to a persistent higher intensity in global proton aurora, also when the IMF $B_z > 0$. The dynamic pressure induced aurora is most intense on the nightside and flanks. (2) The proton aurora intensity responds promptly to variations in the solar wind dynamic pressure. (3) We observe a dawn–dusk asymmetry, with the highest intensity at dusk, which shows that the protons have been subjected to gradient/curvature drift in the magnetosphere. (4) When IMF $B_z < 0$, the effect of high solar wind dynamic pressure is more dramatic, in terms of proton aurora intensity. Any mechanism, or mechanisms, that aim to explain the dynamic pressure proton aurora must account for the above observations.

[39] The relative changes in solar wind density and velocity during some of the events we have studied suggest that Kelvin–Helmholtz waves on the magnetopause are most likely not the cause for the dynamic pressure induced aurora. Our observations suggest that the precipitation is caused by a mechanism directly connected to the compression of the magnetosphere, possibly: (1) Adiabatic energization, (2) increase in the size of the loss cone due to a decrease in mirror ratio, (3) enhanced magnetospheric convection, (4) a reduced curvature radius on the nightside magnetic field lines, (5) interaction with EMIC waves due to increased energy anisotropy, or a combination of these mechanisms.

[40] Since all these mechanisms may be present simultaneously, further study is needed to differentiate between them. Adiabatic energization, increase in the size of the loss cone, and EMIC waves caused by energy anisotropy depend on the relative increase of the magnetic field strength when the magnetosphere is compressed. It is thus expected that these processes are more important at high latitude magnetic field lines, which experience a larger relative increase during compression. In situ measurements of EMIC wave activity during high dynamic pressure could provide further support for this theory. Since the efficiency of the pitch angle scattering on stretched field lines depends on the mass and energy of the particles, the precipitation of energetic protons should increase much more than the electron precipitation where this is the most important mechanism. This could be tested by in situ measurements of particle precipitation. The flank location (two-cell structure) which was particularly prominent in two of the above events (22 April and 25 October), may be an auroral signature of magnetospheric convection during high dynamic pressure, which has received increasing attention in the recent years. A study of the ionospheric convection in these events could provide a test for this hypothesis.

[41] **Acknowledgments.** This study was financed by the IPY-ICESTAR project, The Research Council of Norway, contract 176045/S30. We thank the IMAGE-FUV team and PI S. Mende for the SI-12 data. The geomagnetic data were provided by the WDC for Geomagnetism, Kyoto.

We thank the ACE SWEPAM and MAG instrument teams and the ACE Science Center for providing the ACE data.

[42] Wolfgang Baumjohann thanks Athanasios Boudouridis and another reviewer for their assistance in evaluating this paper.

References

Anderson, B. J., and D. C. Hamilton (1993), Electromagnetic ion cyclotron waves stimulated by modest magnetospheric compressions, *J. Geophys. Res.*, *98*, 11,369–11,382.

Axford, W. I., and C. O. Hines (1961), A unifiying theory of high-latitude geophysical phenomena and geomagnetic storms, *Can. J. Phys.*, *39*, 1433.

Baumjohann, W., and R. A. Treumann (1997), *Advanced Space Plasma Physics*, Imperical College Press, Covent Garden, London.

Boudouridis, A., E. Zesta, L. R. Lyons, P. C. Anderson, and D. Lummerzheim (2003), Effect of solar wind pressure pulses on the size and strength of the auroral oval, *J. Geophys. Res.*, *108*(A4), 8012, doi:10.1029/2002JA009373.

Boudouridis, A., E. Zesta, L. R. Lyons, P. C. Anderson, and D. Lummerzheim (2004), Magnetospheric reconnection driven by solar wind pressure fronts, *Ann. Geophys.*, *22*, 1367–1378.

Boudouridis, A., E. Zesta, L. R. Lyons, P. C. Anderson, and D. Lummerzheim (2005), Enhanced solar wind geoeffectiveness after a sudden increase in dynamic pressure during southward IMF orientation, *J. Geophys. Res.*, *110*, A05214, doi:10.1029/2004JA010704.

Boudouridis, A., E. Zesta, L. R. Lyons, P. C. Anderson, and A. J. Ridley (2008), Temporal evolution of the transpolar potential after a sharp enhancement in solar wind dynamic pressure, *Geophys. Res. Lett.*, *35*, L02101, doi:10.1029/2007GL031766.

Burton, R. K., R. L. McPherron, and C. T. Russell (1975), An empirical relationship between interplanetary conditions and *Dst*, *J. Geophys. Res.*, *81*, 4204–4214.

Coumans, V., J.-C. Gérard, B. Hubert, and M. Meurant (2006), Global auroral proton precipitation observed by IMAGE-FUV: Noon and midnight brightness dependence on solar wind characteristics and IMF orientation, *J. Geophys. Res.*, *111*, A05210, doi:10.1029/2005JA011317.

Craven, J. D., L. A. Frank, C. T. Russel, E. E. Smith, and R. P. Lepping (1986), Global auroral responses to magnetospheric compressions by shocks in solar wind: Two case studies, in *Solar Wind-Magnetospheric Coupling*, edited by Y. Kamide and J. A. Slavin, pp. 377–380, Terra Sci., Tokyo.

Dungey, J. W. (1961), Interplanetary magnetic field and the auroral zones, *Phys. Rev.*, 6, 47–48.

Engebretson, M., K.-H. Glassmeier, M. Stellmacher, W. J. Hughes, and H. Lühr (1998), The dependence of high-latitude Pc5 wave power on solar wind velocity and on the phase of high-speed solar wind streams, *J. Geophys. Res.*, *103*, 26,271–26,283.

Frey, H. U., S. B. Mende, V. Angelopoulos, and E. F. Donovon (2004), Substorm onset observations by IMAGE-FUV, *J. Geophys. Res.*, *109*, A10304, doi:10.1029/2004JA010607.

Frey, H. U., et al. (2003), Summary of quantitative interpretation of IMAGE far ultraviolet auroral data, *Space Sci. Rev.*, *109*, 255–283.

Gérard, J., B. Hubert, M. Meurant, V. I. Shematovich, D. V. Bisikalo, H. Frey, S. Mende, G. R. Gladstone, and C. W. Carlson (2001), Observation of the proton aurora with IMAGE FUV imager and simultaneous ion flux in situ measurements, *J. Geophys. Res.*, *106*, 28,939–28,948.

Hardy, D. A., M. S. Gussenhoven, and D. Brautigam (1989), A statistical model of auroral ion precipitation, *J. Geophys. Res.*, *94*, 370–392.

Lee, D.-Y., and L. R. Lyons (2004), Geosynchronous magnetic field response to solar wind dynamic pressure pulse, *J. Geophys. Res.*, *109*, A04201, doi:10.1029/2003JA010076.

Lee, D.-Y., S. Ohtani, P. C. Brandt, and L. R. Lyons (2007), Energetic neutral atom response to solar wind dynamic pressure enhancements, *J. Geophys. Res.*, *112*, A09210, doi:10.1029/2007JA012399.

Liou, K., P. T. Newell, T. Sotirelis, and C.-I. Meng (2006), Global auroral response to negative pressure impulses, *Geophys. Res. Lett.*, *33*, L11103, doi:10.1029/2006GL025933.

Liou, K., P. T. Newell, J.-H. Shue, C.-I. Meng, Y. Miyashita, H. Kojima, and H. Matsumoto (2007), "Compression aurora": Particle precipitation driven by long-duration high solar wind ram pressure, *J. Geophys. Res.*, *112*, A11216, doi:10.1029/2007JA012443.

Lukianova, R. (2003), Magnetospheric response to sudden changes in solar wind dynamic pressure inferred from polar cap index, *J. Geophys. Res.*, *108*(A12), 1428, doi:10.1029/2002JA009790.

Mende, S. B., H. U. Frey, T. J. Immel, D. G. Mitchell, P. C. Brandt, and J. C. Gérard (2002), Global comparison of magnetospheric ion fluxes and auroral precipitation during a substorm, *Geophys. Res. Lett.*, *29*(12), 1609, doi:10.1029/2001GL014143.

Mende, S. B., H. U. Frey, T. J. Immel, J.-C. Gérard, B. Hubert, and S. A. Fuselier (2003), Global imaging of proton and electron aurorae in the far ultraviolet, *Space Sci. Rev.*, *109*, 211–254.

Mende, S. B., et al. (2000), Far ultraviolet imaging from the IMAGE spacecraft. 3. Spectral imaging of Lyman-α and OI 135.6 nm, *Space Sci. Rev.*, *91*, 287–318.

Meurant, M., J.-C. Gérard, B. Hubert, V. Coumans, C. Blockx, N. Østgaard, and S. B. Mende (2003), Dynamics of global scale electron and proton precipitation induced by a solar wind pressure pulse, *Geophys. Res. Lett.*, *30*(20), 2032, doi:10.1029/2003GL018017.

Meurant, M., J.-C. Gérard, C. Blockx, B. Hubert, and V. Coumans (2004), Propagation of electron and proton shock-induced aurora and the role of the interplanetary magnetic field and solar wind, *J. Geophys. Res.*, *109*, A10210, doi:10.1029/2004JA010453.

Sergeev, V. A., E. M. Sazhina, N. A. Tsyganenko, and F. Søraas (1983), Pitch-angle scattering of energetic protons in the magnetotail current sheet as the dominant source of their isotropic precipitation into the nightside ionosphere, *Planet. Space Sci.*, *31*, 1147–1155.

Shue, J.-H., P. T. Newell, K. Liou, C.-I. Meng, Y. Kamide, and R. P. Lepping (2002), Two-component aurora, *Geophys. Res. Lett.*, *29*(10), 1379, doi:10.1029/2002GL014657.

Søraas, F., K. Aarsnes, K. Oksavik, and D. S. Evans (2002), Ring current intensity estimated from low-altitude proton observations, *J. Geophys. Res.*, *107*(A7), 1149, doi:10.1029/2001JA000123.

Spann, J. F., M. Brittnacher, R. Elsen, G. A. Germany, and G. K. Parks (1998), Initial response and complex polar cap structures of the aurora in response to the January 10, 1997 magnetic cloud, *Geophys. Res. Lett.*, *25*, 2577–2580.

Vorobyev, V. G. (1974), SC-associated effects in auroras, *Geomagn. Aeron.*, *14*, 72–74.

Wanliss, J. A., and K. M. Showalter (2006), High-resolution global storm index: *Dst* versus SYM-H, *J. Geophys. Res.*, *111*, A02202, doi:10.1029/2005JA011034.

Zhou, X.-Y., and B. T. Tsurutani (1999), Rapid intensification and propagation of the dayside aurora: Large scale interplanetary pressure pulses (fast shocks), *Geophys. Res. Lett.*, *26*, 1097–1100.

Zhou, X.-Y., and B. T. Tsurutani (2003), Dawn and dusk auroras caused by gradual, intense solar wind ram pressure events, *J. Atmos. Terr. Phys.*, *66*, 153–160, doi:10.1016/j.jastp.2003.09.008.

Zhou, X.-Y., R. J. Strangeway, P. C. Anderson, D. G. Sibeck, B. T. Tsurutani, G. Haerendel, H. U. Frey, and J. K. Arballo (2003), Shock aurora: FAST and DMSP observations, *J. Geophys. Res.*, *108*(A4), 8019, doi:10.1029/2002JA009701.

K. M. Laundal and N. Østgaard, Department of Physics and Technology, University of Bergen, Allégaten 55, N-5007 Bergen, Norway. (karl.laundal@ift.uib.no; nikolai.ostgaard@ift.uib.no)